A Theoretical Study on the Potential Energy Surface of the $^3C_2$ + NO Reaction

Zhi-Gang Wei,[†] Xu-Ri Huang,*[,†] Shao-Wen Zhang,[‡] Yan-Bo Sun,[†] Hu-Jun Qian,[†] and Chia-Chung Sun[†]

Institute of Theoretical Chemistry, State Key Laboratory of Theoretical and Computational Chemistry, Jilin University, Changchun 130023, People's Republic of China, and School of Chemical Engineering and Materials Science, Beijing Institute of Technology, Beijing 100081, People's Republic of China

Received: March 14, 2004; In Final Form: May 29, 2004

The reaction of $^3C_2$ radical with NO molecule is studied at the B3LYP/6-311G(d) level of theory. Both doublet and quartet potential energy surfaces (PES) are considered. On the doublet potential energy surface, we obtain four major pathways in which the pathways $^3C_2$ + NO ⇌ **1** CCNO → **2** (NC)CO → **3** CNCO → $\mathbf{P_1}$ CN + CO and $^3C_2$ + NO ⇌ **1** → **4** CC(NO) → **2** → **3** → $\mathbf{P_1}$ CN + CO have lower energetics than the other two pathways that form the ^{3}O atom, namely $^3C_2$ + NO ⇌ **1** CCNO → $\mathbf{P_2}$ ^{3}O + ^{2}CCN and $^3C_2$ + NO ⇌ **1** CCNO → **5** ON(CC) → $\mathbf{P_3}$ ^{3}O + $^2CCN_{ring}$. However, the latter two pathways may compete with the former two pathways. The calculated energetics of the four pathways may account for the experimental results that CN is the primary product at low temperatures and ^{3}O is the main product at higher temperatures. The barrierless entrance to the first adduct isomer **1** and the tight transition states to the products $\mathbf{P_1}$, can provide a reasonable explanation for the experimentally observed negative temperature dependence of rate constants at low temperatures. The pathways on the quartet potential energy surface are less competitive than those on the doublet potential energy surface. Thus, they are negligible.

1. Introduction

C_2 radicals play an important role in the combustion process[1−3] as well as in interstellar chemistry.[4,5] The reaction of $^3C_2$ radical with nitric oxide, which can be seen as one of the important reactions in combustion and the nitric oxide reburning process, has been investigated by many previous investigators.[6−14]

Reisler et al.[6,7] studied the $^3C_2$ + NO reaction extensively at room temperature. They suggested the four-center single-step reaction as follows:

$$C_2(a^3\Pi) + NO(X^2\Pi) \rightarrow CN\ (A^2\Pi, B^2\Sigma) + CO(X^1\Sigma) \quad (1)$$

The standard reaction enthalpy at 298 K ($\Delta H°_{298}$) for this reaction is −119.8 and −72.5 kcal mol^{-1} respectively for the formation of states A and B.[15−17] Their result was in accord with the crossed molecular beams study by Krause.[8] In a spectroscopic study on nitric oxide−acetylene flame, Le et al.[9] also realized that the reaction of C_2 with NO is "extremely fast" and accepted the conclusion of Reisler et al.[6,7] and Krause.[8]

However, in the study of the effect of NO on different hydrocarbon flames, Williams et al.[10] found that the measured C_2 concentration and the influence of C_2 on the NO concentration could not be described satisfactorily with the four-center reaction mechanism. Subsequently, Kruse et al.[11] studied the reaction in a high-temperature range (3150−3950 K). According to their product formation measurements of O, N, and CN, they proposed the reactions as follows:

$$^3C_2 + NO \rightarrow C_2N + O\ \Delta H°_{298}\ (\text{ref } 18) \quad (2)$$

$$^3C_2 + NO \rightarrow C_2OH + N\ \Delta H°_{298} = -15.3\ \text{kcal mol}^{-1}\ (\text{refs } 15,19) \quad (3)$$

For this discrepancy, Becker et al.[12,13] stated that further studies of the primary products and their temperature dependence would be helpful to elucidate the reaction mechanism. Recently, Ristanovic et al.[14] studied the reaction in a wide temperature range (292−968 K). They confirmed that there should be a mechanism change between the high (3150−3950 K) and the low (292−968 K) temperature ranges.

On the basis of the results of the previous investigators, it seems that a detailed theoretical characterization on the potential-energy surface of the $^3C_2$ + NO reaction is very desirable. Therefore, an attempt is made in the present contribution to elucidate the mechanism of the reaction. Some conclusions that are made in this work may be helpful for further theoretical and experimental studies of this reaction.

2. Computational Methods

All calculations are carried out using the Gaussian 98 program.[20] The geometries of the reactants, the products, the intermediate isomers, and the transition states are optimized using the hybrid density functional B3LYP method with the 6-311G(d) basis set. To confirm that each transition state correctly connects to the corresponding species, we also perform intrinsic reaction coordinate (IRC) calculations at the B3LYP/6-311G(d) level of theory. The single-point energies are calculated at the CCSD(T)/6-311G(d) level of theory. In

* Corresponding author. Fax: 86-431-8945942. E-mail address: Weizg2002@yahoo.com.cn.

† Institute of Theoretical Chemistry, State Key Laboratory of Theoretical and Computational Chemistry, Jilin University.

‡ School of Chemical Engineering and Materials Science, Beijing Institute of Technology.

10.1021/jp048868p CCC: $27.50
Published on Web 07/16/2004

TABLE 1: Relative Energies and ZPE (in kcal/mol) for the Stationary Points Involved in the $^3C_2$ + NO Reaction

species	ZPE[a]	B3LYP/ 6-311G(d)[b]	CCSD(T)/ 6-311G(d)[c]	species	ZPE[a]	B3LYP/ 6-311G(d)[b]	CCSD(T)/ 6-311G(d)[c]
R ($^3C_2$ + NO)	5.3	0.0	0.0	TS1-2	5.9	−17.3	−14.4
P_1 (CN + CO)	6.2	−136.9	−140.8	TS2-3	7.3	−129.3	−121.6
P_2 (^{3}O + ^{2}CCN)	5.4	−3.7	−2.9	TS3-P_1	6.6	−132.2	−128.3
P_3 (^{3}O + ^{2}CCN$_{ring}$)	4.5	8.7	7.8	TS1-4	6.0	−26.8	−13.9
P_4 (^{2}N + ^{1}CCO)	5.6	2.7	−4.8	TS4-2	5.7	−21.3	−7.7
P_5 (^{2}N + ^{3}CCO)	5.6	−22.5	−24.8	TS1-5	7.4	−44.6	−31.4
P_6 (^{4}OCCN)	7.5	−93.3	−74.2	TSR-6	5.7	1.9	9.4
1 CCNO	7.9	−77.1	−60.2	TS6-P_4	5.4	13.2	17.9
2 (NC)CO	8.8	−143.5	−133.2	TS6-4	5.9	−6.2	5.6
3 CNCO	8.4	−155.3	−145.5	^{4}TSR-1	5.8	1.6	6.1
4 CC(NO)	7.0	−34.9	−25.1	^{4}TS1-P_2	5.5	−1.0	8.6
5 ON(CC)	8.0	−56.1	−41.4	^{4}TSR-2	5.3	16.6	28.3
6 CCON	6.8	−20.1	−5.9	^{4}TS2-P_5	5.6	−0.8	10.6
^{4}1 CCNO	7.8	−42.1	−24.7	^{4}TS2-3	5.7	−2.9	9.4
^{4}2 CCON	6.6	−10.3	−0.2	^{4}TS3-4	5.9	−6.1	4.6
^{4}3 CC(ON)	6.7	−15.9	−4.5	^{4}TS4-P_6	6.0	−33.4	−21.2
^{4}4 CC(O)N	6.6	−41.6	−29.7				

[a] ZPE is calculated at the B3LYP/6-311G(d) level of theory. [b] Including ZPE correction. [c] Calculated based on the geometries optimized at the B3LYP/6-311G(d) level of theory; ZPEs at the B3LYP/6-311G(d) level of theory are included.

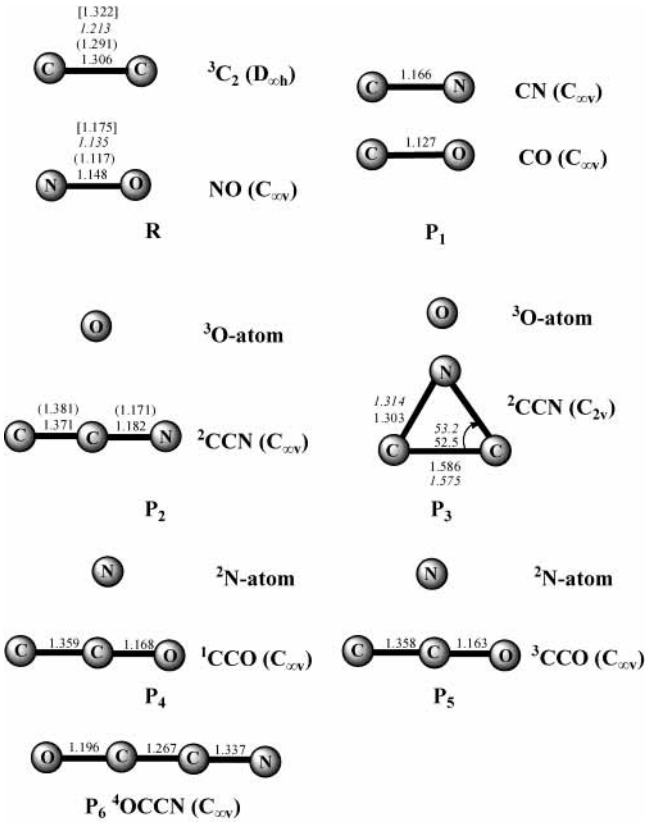

Figure 1. Optimized geometries [Å, deg] of the reactants and the products for the $^3C_2$ + NO reaction. Numbers in roman type show the structures at the B3LYP/6-311G(d) level of theory. The numbers in parentheses show the structures at the HF/6-311G(d) level of theory. The numbers in italics show the structures at the MP2/6-311G(d) level of theory. The numbers in brackets show the structures at the QCISD/6-31G(d) level of theory.

addition, the HF, MP2, and QCISD methods are used to calculate and check some stable and transition geometry structures.

3. Results and Discussion

The optimized structural parameters of the reactants and the products for the $^3C_2$ + NO reaction are shown in Figure 1; the optimized structural parameters of the isomers and the transition states on the doublet electronic state are shown in Figure 2; the optimized structural parameters of the isomers and the transition states on the quartet electronic state are shown in Figure 3. In Figures 1−3, the numbers in roman type denote the structures optimized at the B3LYP/6-311G(d) level of theory, the numbers in parentheses denote the structures optimized at the HF/6-311G(d) level of theory, italicized numbers denote the structures optimized at the MP2/6-311G(d) level of theory, and the numbers in brackets show the structures at the QCISD/6-31G(d) level of theory. The total energies of all the species involved in the reaction are listed in Table 1. Figures 4 and 5 show schematic plots of the relative energies of the doublet and quartet potential energy surfaces (PES), respectively.

3.1. The Doublet Potential Energy Surface. As can be seen from Figure 4, there are four products, six intermediate isomers, and nine transition states present on the doublet potential energy surface. The corresponding optimized geometries and energies are shown in Figures 1−2 and Table 1.

There are two distinguishable reaction mechanisms involved in the $^3C_2$ + NO reaction on the doublet potential energy surface. The N-atom attacking mechanism starts from the attack of the N-atom of the NO molecule to the C-atom of the $^3C_2$ radical in the first reaction step; the O-atom attacking mechanism starts from the attacking of the O-atom of the NO molecule to the C-atom of the $^3C_2$ radical in the first reaction step. We should mention that we also tried to find the direct N-atom and O-atom elimination mechanisms but failed in finding them.

3.1.A. N-Atom Attacking Mechanism. The first step of this mechanism involves the N-atom of the NO molecule directly attacking the C-atom of the $^3C_2$ radical to form the adduct isomer **1** CCNO. As shown in Figure 4, this is a barrierless exothermic step with the reaction energy of −60.2 kcal mol^{-1} at the CCSD(T)/6-311G(d)//B3LYP/6-311G(d)+ZPE level of theory. On the other hand, we find a weakly bound complex **C** and a transition state **TSC-1** for this step at the HF/6-311G(d) level of theory (see Figure 2 for geometries). Both **C** and **TSC-1** lie below the reactants $^3C_2$ + NO, and the conversion barrier of **C** to **1** is just 2.4 kcal/mol at the HF/6-311G(d) level of theory. However, when we reoptimize **C** and **TSC-1** at higher levels of theory such as MP2 and QCISD, both the complex **C** and transition state **TSC-1** vanish. In fact, they may be the artifacts of the highly spin-contaminated HF level because the $\langle S^2 \rangle$ value is 1.98 for **C** and 2.44 for **TSC-1**, while the value for a pure doublet state should be 0.75. This implies that there might be no such complex and transition state. From the adduct isomer **1** CCNO, there are four isomerization and dissociation pathways

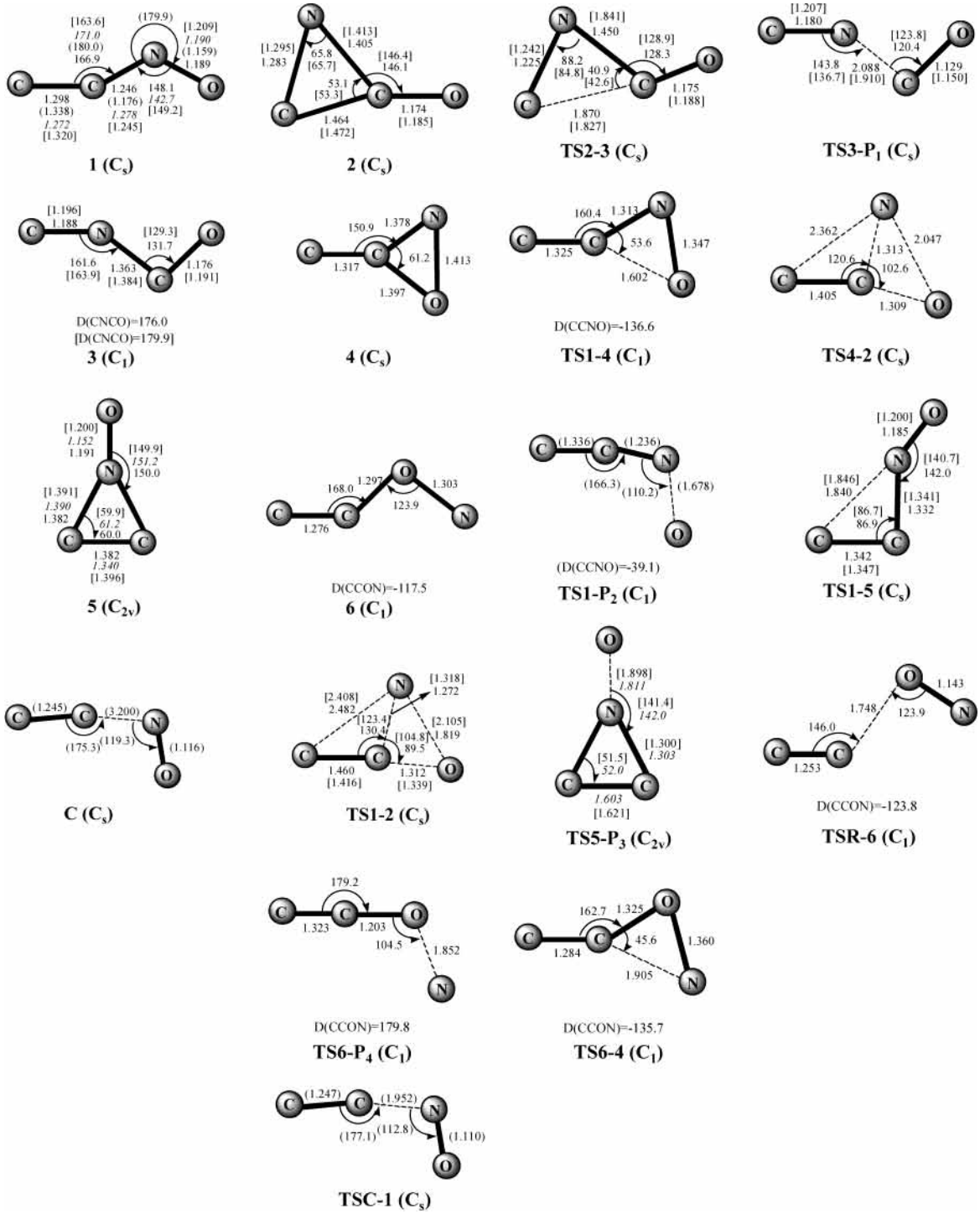

Figure 2. Optimized geometries [Å, deg] of the doublet isomers and the transition states for the $^3C_2$ + NO reaction. Numbers in roman type show the structures at the B3LYP/6-311G(d) level of theory. The numbers in parentheses show the structures at the HF/6-311G(d) level of theory. The numbers in italics show the structures at the MP2/6-311G(d) level of theory. The numbers in brackets show the structures at the QCISD/6-31G(d) level of theory. D(abcd) denotes the dihedral angle between the abc and bcd plans.

that can be expressed as follows:

Path RP$_1$(1): R $^3C_2$ + NO → **1** CCNO → **2** (NC)CO → **3** CNCO → **P$_1$** CN + CO

Path RP$_1$(2): R → 1 → 4 CC(NO) → **2** → **3** → **P$_1$** CN+CO

Path RP$_2$(1): R → 1 → P$_2$ ^{3}O + ^{2}CCN

Path RP$_3$(1): R → 1 → 5 ON(CC) → **P$_3$** O + ^{2}CCN$_{ring}$

Clearly, from the isomer **1** CCNO with the energy of −60.2 kcal mol^{-1}, the pathway **RP$_1$(1)** can reach the products **P$_1$** CN + CO easily by going through **TS1-2**, isomer **2** (NC)CO, **TS2-3**, isomer **3** CNCO, and **TS3-P$_1$** in succession with the energies of −14.4, −133.2, −121.6, −145.5, and −128.3 kcal mol^{-1}, respectively. Since all the energies of the transition states and isomers in the pathway **RP$_1$(1)** are lower than that of the reactants, the rate of this pathway should be very fast. Furthermore, since the pathway **RP$_1$(1)** has no transition state in the first reaction step and tight structure isomers and transition

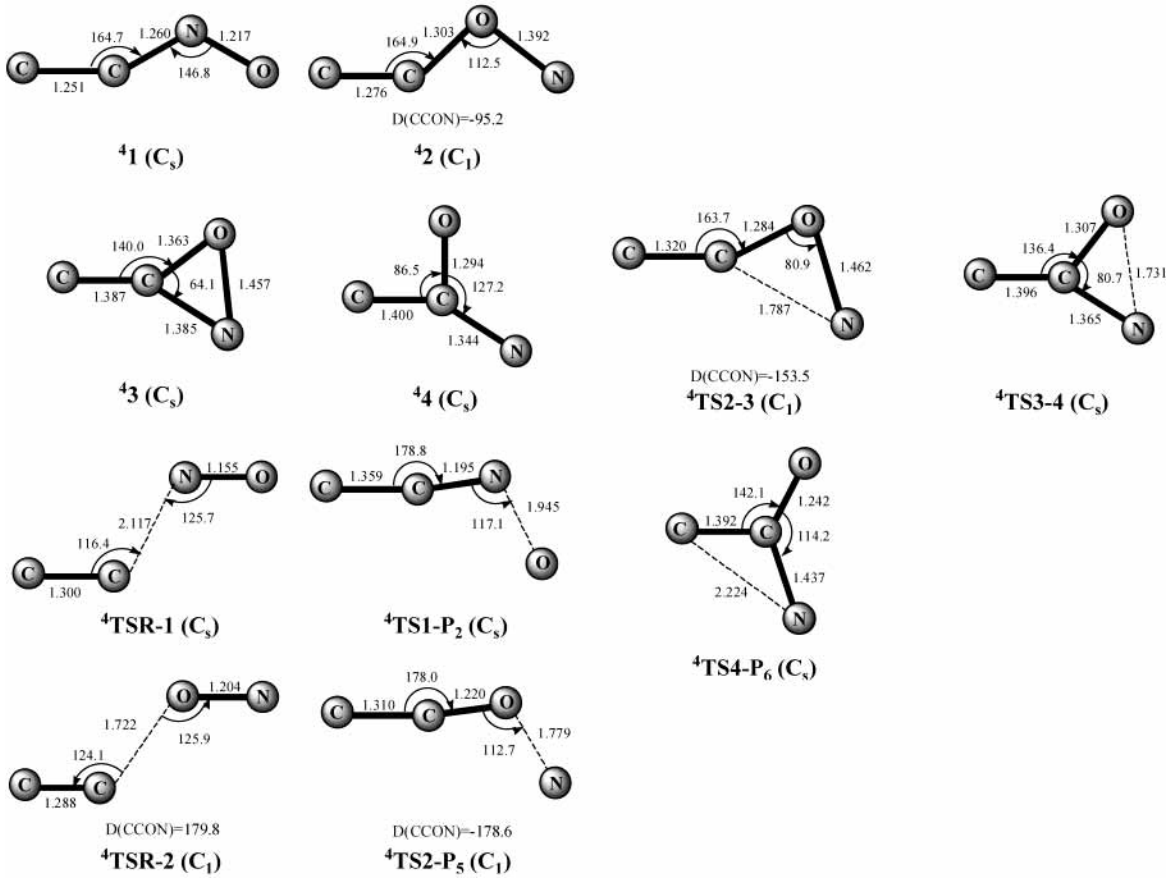

Figure 3. Optimized geometries [Å, deg] of the quartet isomers and the transition states for the $^3C_2$ + NO reaction at the B3LYP/6-311G(d) level of theory. D(abcd) denotes the dihedral angle between the abc and bcd plans.

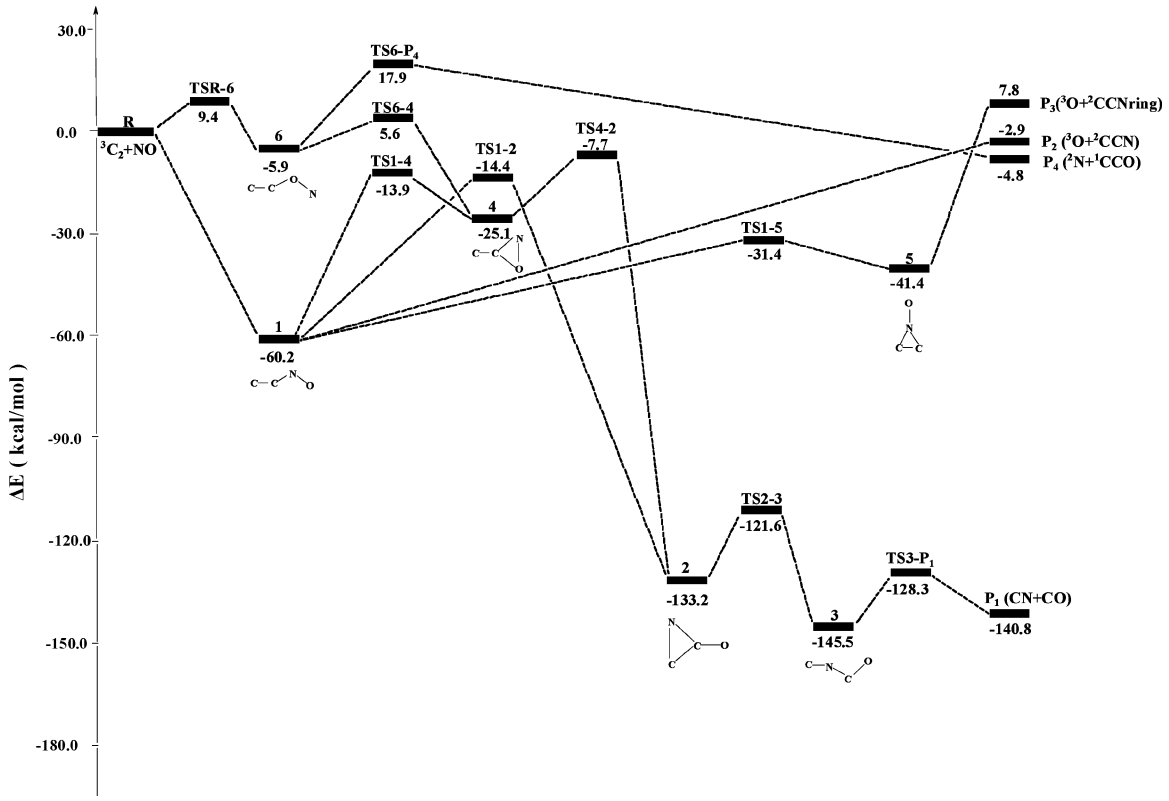

Figure 4. Doublet potential energy surface (PES) for the $^3C_2$ + NO reaction at the CCSD(T)/6-311G(d)//B3LYP/6-311G(d)+ZPE level of theory.

states to the products, this pathway should possess the character of negative temperature dependence, which can account for the experimental results in low-temperature ranges (T < 968 K).[14]

It is obvious that pathway **RP$_1$(2)** is similar to pathway **RP$_1$-(1)**. Thus, pathway **RP$_1$(2)** may also have negative temperature dependence in low-temperature ranges (T < 968 K).[14] Pathway

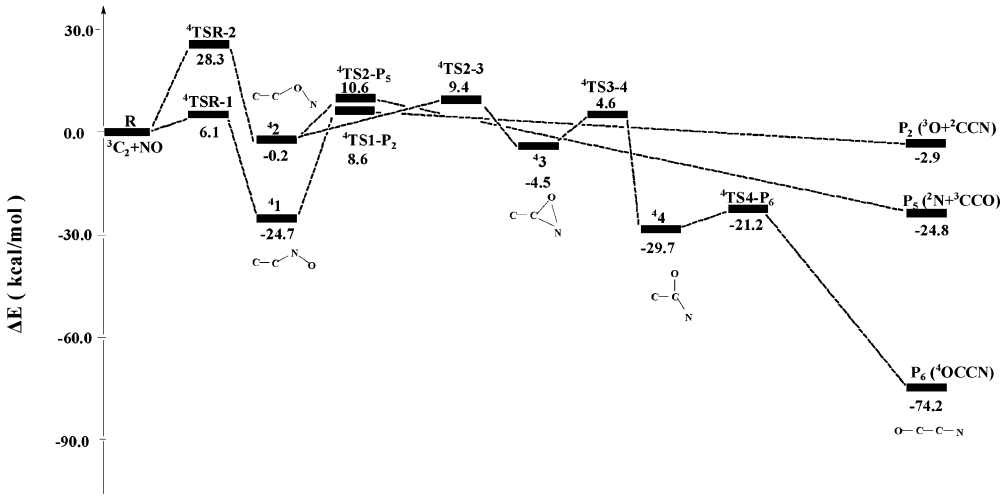

Figure 5. Quartet potential energy surface (PES) for the $^3C_2$ + NO reaction at the CCSD(T)/6-311G(d)//B3LYP/6-311G(d)+ZPE level of theory.

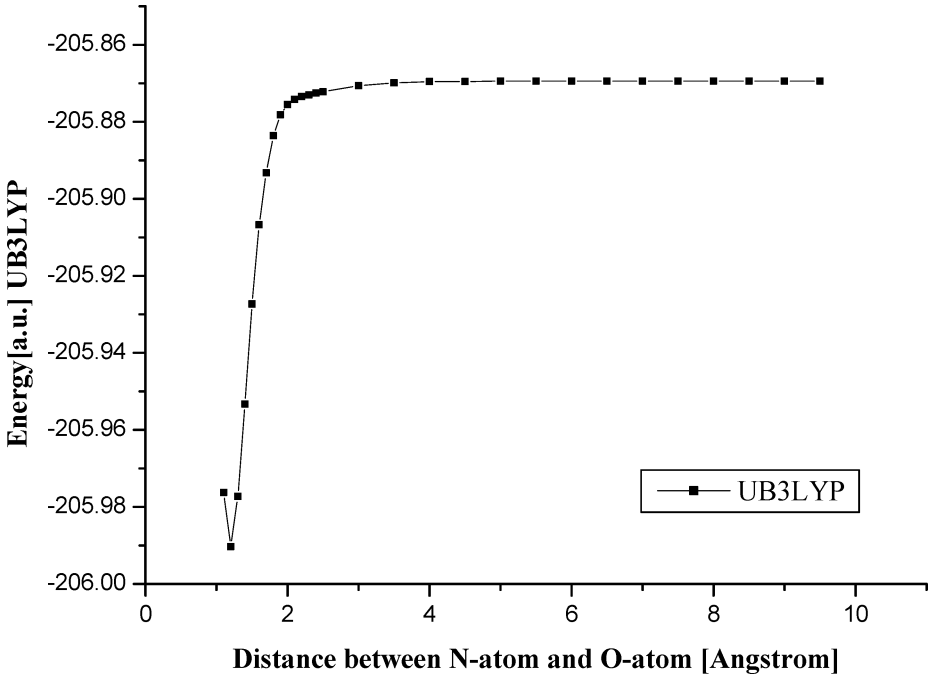

Figure 6. Dissociation curve with respect to the dissociation of the N−O bond in the isomer **1** CCNO at the UB3LYP/6-311G(d) level of theory.

RP$_1$(2) has the same steps of **R** → **1**, **2** → **3**, and **3** → **P$_1$** as pathway **RP$_1$(1)**. The difference of the two pathways is how isomer **1** is changed to isomer **2**. In pathway **RP$_1$(1)**, isomer **1** forms isomer **2** via the transition state **TS1-2** with the energy of −14.4 kcal mol^{-1}, whereas in pathway **RP$_1$(2)** isomer **1** forms isomer **2** by passing **TS1-4**, isomer **4**, and **TS4-2** successively with the energies of −13.9, −25.1, and −7.7 kcal mol^{-1}, respectively. The difference of the two pathways may lead us to the fact that pathway **RP$_1$(1)** is more favorable than pathway **RP$_1$(2)**.

For pathway **RP$_2$(1)**, isomer **1** CCNO transforms to products **P$_2$** ^{3}O + ^{2}CCN directly. The dissociation curve of the N−O bond in isomer **1** CCNO to approach the products **P$_2$** ^{3}O + ^{2}CCN is worked out at the UB3LYP/ 6-311G(d) level of theory via point-wise optimization (see Figure 6). We also find the structure of **TS1-P$_2$** at the HF/6-311G(d) level of theory with a loose structure (the N−O bond is as long as 1.678 Å in Figure 2). However, optimization of **TS1-P$_2$** at MP2 and QCISD levels fails, which always leads to the separate fragments **P$_2$**. Thus, we may conclude that there is no barrier in pathway **RP$_2$(1)** either from the reactants **R** $^3C_2$ + NO to isomer **1** or from isomer **1** to products **P$_2$** ^{3}O + ^{2}CCN. We can see from Table 1 that the energy of products **P$_2$** is higher than that of transition states **TS1-2** −14.4 kcal mol^{-1}, **TS1-4** −13.9 kcal mol^{-1} and **TS4-2** −7.7 kcal mol^{-1} in pathways **RP$_1$(1)** and **RP$_1$(2)**. Pathway **RP$_2$-(1)** should be less competitive than pathways **RP$_1$(1)** and **RP$_1$-(2)** in low-temperature range.

For pathway **RP$_3$(1)**, isomer **1** CCNO −60.2 kcal mol^{-1} transforms to isomer **5** ON(CC) −41.4 kcal mol^{-1} via transition state **TS1-5** with the relative energy of −31.4 kcal mol^{-1}, and subsequently, isomer **5** transforms to products **P$_3$** ^{3}O + ^{2}CCN$_{ring}$ 7.8 kcal mol^{-1} barrierlessly. The dissociation curve of the N−O bond in isomer **5** ON(CC) to approach the products **P$_3$** ^{3}O + ^{2}CCN$_{ring}$ is worked out at the UB3LYP/6-311G(d) level via point-wise optimization (see Figure 7). At the MP2/6-311G(d) level of theory, **TS5-P$_3$** is found with a loose structure (see Figure 2). The dissociation barrier of **5** to **P$_3$** and the association barrier of **P$_3$** to **5** are 46.3 and 1.7 kcal mol^{-1}, respectively, at the CCSD(T)/6-311G(d)//MP2/6-311G(d)+ZPE level of theory. Since the energy of the products **P$_3$** ^{3}O + ^{2}CCN$_{ring}$ 7.8 kcal mol^{-1} is much higher than the energies of the transition states **TS1-2** −14.4 kcal mol^{-1}, **TS1-4** −13.9 kcal mol^{-1}, **TS4-2** −7.7

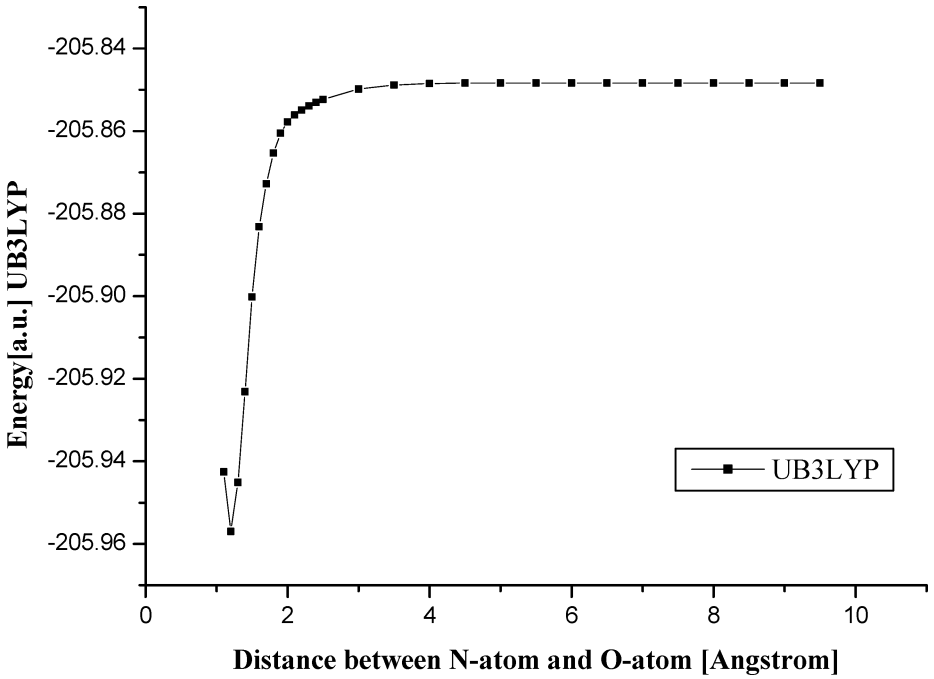

Figure 7. Dissociation curve with respect to the dissociation of the N−O bond in the isomer **5** ON(CC) at the UB3LYP/6-311G(d) level of theory.

kcal mol^{-1}, and $\mathbf{P_2}$ −2.9 kcal mol^{-1} in the pathways $\mathbf{RP_1(1)}$, $\mathbf{RP_1(2)}$, and $\mathbf{RP_2(1)}$. Pathway $\mathbf{RP_3(1)}$ should be less competitive than pathways $\mathbf{RP_1(1)}$, $\mathbf{RP_1(2)}$ and $\mathbf{RP_2(1)}$ in low-temperature range.

3.1.B. O-Atom Attacking Mechanism. For the first reaction step **R** → **6**, the O-atom of the NO molecule attacks the C-atom of the $^3C_2$ radical to form isomer **6** CCON with the energy of −5.9 kcal mol^{-1} via the transition state **TSR-6** with a high entrance barrier of 9.4 kcal mol^{-1}. For the two distinguishable second steps, **6** → $\mathbf{P_4}$ and **6** → **4**, $\mathbf{TS6\text{-}P_4}$ is associated with the high relative energy of 17.9 kcal mol^{-1}, and **TS6-4** is associated with the high relative energy of 5.6 kcal mol^{-1}. The high relative energy transition states in the first and second steps in the O-atom attacking mechanism may rule out their significance in atmospheric chemistry at lower temperature, and even at higher temperatures. For conciseness, we only list them as follows:

Path $\mathbf{RP_4(1)}$: **R** $^3C_2$ + NO → **6** CCON → $\mathbf{P_4}$ ^{2}N + ^{1}CCO

Path $\mathbf{RP_1(3)}$: **R** → **6** → **4** CC(NO) → **2** (NC)CO → **3** CNCO → $\mathbf{P_1}$ CN + CO

Path $\mathbf{RP_1}$ (4): **R** → **6** → **4** → **1** CCNO → **2** → **3** → $\mathbf{P_1}$ CN + CO

Path $\mathbf{RP_2(2)}$: **R** → **6** → **4** → **1** → $\mathbf{P_2}$ ^{3}O + ^{2}CCN

Path $\mathbf{RP_2(3)}$: **R** → **6** → **4** → **2** → **1** → $\mathbf{P_2}$ ^{3}O + ^{2}CCN

Path $\mathbf{RP_3(2)}$: **R** → **6** → **4** → **1** → **5** ON(CC) → $\mathbf{P_3}$ O + ^{2}CCN$_{ring}$

Path $\mathbf{RP_3(3)}$: **R** → **6** → **4** → **2** → **1** → **5** → $\mathbf{P_3}$ O + ^{2}CCN$_{ring}$

3.2. The Quartet Potential Energy Surface. There are three pathways that can be seen on the quartet potential energy surface as follows:

Path $\mathbf{RP_2(4)}$: **R** $^3C_2$ + NO → ^{4}**1** CCNO → $\mathbf{P_2}$ ^{3}O + ^{2}CCN

Path $\mathbf{RP_5(1)}$: **R** $^3C_2$ + NO → ^{4}**2** CCON → $\mathbf{P_5}$ ^{2}N + ^{3}CCO

Path $\mathbf{RP_6(1)}$: **R** → ^{4}**2** → ^{4}**3** CC(ON) → ^{4}**4** CC(O)N → $\mathbf{P_6}$ ^{4}OCCN

In pathway $\mathbf{RP_2(4)}$, the N-atom of the NO molecule attacks the C-atom of the $^3C_2$ radical in the first reaction step to form isomer ^{4}**1** CCNO −24.7 kcal mol^{-1} via transition state ^{4}**TSR-1** 6.1 kcal mol^{-1}. Then the isomer ^{4}**1** transforms to the products $\mathbf{P_2}$ ^{3}O + ^{2}CCN −2.9 kcal mol^{-1} via the transition state $^4\mathbf{TS1\text{-}P_2}$ 8.6 kcal mol^{-1}. The high relative energies of ^{4}**TSR-1** 6.1 kcal mol^{-1} and $^4\mathbf{TS1\text{-}P_2}$ 8.6 kcal mol^{-1} may make the pathway $\mathbf{RP_2(4)}$ less competitive in the reaction.

Pathways $\mathbf{RP_5(1)}$ and $\mathbf{RP_6(1)}$ may be not competitive in the reaction, for transition state ^{4}**TSR-2** with a high energy of 28.3 kcal mol^{-1} in the first reaction step effectively blocks the pathways to go through the subsequent steps.

Finally, for eight dominant structures **1**, **2**, **3**, **4**, **TS1-2**, **TS2-3**, $\mathbf{TS3\text{-}P_1}$, and **TS1-5**, we have carried out the cost-expensive geometrical calculations at the QCISD/6-31G(d) level of theory to test the reliability of the present DFT-based calculations. Fortunately, we find that the obtained bond lengths and bond angles are generally in good agreement with the B3LYP/6-311G(d) values, as shown in Figure 2. This indicates that the B3LYP/6-311G(d) method can safely be used for the study of the $^3C_2$ + NO system.

4. Conclusions

The mechanism for the $^3C_2$ + NO reaction is elucidated by means of ab initio MO calculations at the B3LYP/6-311G(d) level of theory. The major pathways in the lower-temperature

range are **RP$_1$(1)** and **RP$_1$(2)** on the doublet potential energy surface and can be expressed as

Path RP$_1$(1): **R** $^3C_2$ + NO → **1** CCNO →
2 (NC)CO → **3** CNCO → **P$_1$** CN + CO

Path RP$_1$(2): **R** → **1** → **4** CC(NO) → **2** → **3** →
P$_1$ CN + CO

In the higher-temperature range, pathways **RP$_2$(1)** and **RP$_3$(1)** on the doublet potential energy surface may be more competitive and can be expressed as

Path RP$_2$(1): **R** → **1** → **P$_2$** ^{3}O + ^{2}CCN

Path RP$_3$(1): **R** → **1** → **5** ON(CC) → **P$_3$** ^{3}O + ^{2}CCN$_{ring}$

Other pathways on the doublet and quartet potential energy surfaces may be less competitive in this reaction.

Pathways **RP$_1$(1)** and **RP$_1$(2)** can fit well with the experimental results in the lower-temperature range, and pathways **RP$_2$(1)** and **RP$_3$(1)** may give an explanation for the experimentally observed O-atom concentration in the higher temperature range. While no pathways can give an explanation for the experimentally observed N-atom concentration in the higher-temperature range, further theoretical and experimental studies are still desirable.

Acknowledgment. This work is supported by the National Natural Science Foundation of China (G29892168, 20073014, 20103003), Doctor Foundation by the Ministry of Education, Foundation for University Key Teacher by the Ministry of Education, and Key Subject of Science and Technology by the Ministry of Education of China_Excellent Young Teacher Foundation of Ministry of Education of China.

References and Notes

(1) Gaydon, A. G.; Wolfhard, H. G. *Flames, Their Structure, Radiation, and Temperature*; Chapman & Hall: New York, 1979.
(2) O'Brien, S. C.; Heath, J. R.; Curl, R. F.; Smalley, R. E. *J. Chem. Phys.* **1988**, *88*, 220.
(3) Perry, M. D.; Raff, L. M. *J. Phys. Chem.* **1994**, *98*, 4375.
(4) Weltner, J. W.; Van Zee, R. *Chem. Rev.* **1989**, *89*, 1713.
(5) Kaiser, R. I. *Chem. Rev.* **2002**, *102*, 1309.
(6) Reisler, H.; Mangir, M.; Wittig, C. *J. Chem. Phys.* **1979**, *71*, 2109.
(7) Reisler, H.; Mangir, M. S.; Wittig, C. *J. Chem. Phys.* **1980**, *73*, 2280.
(8) Krause, H. F. *J. Chem. Phys.* **1979**, *70*, 3871.
(9) Le, Q. N.; Vanpee, M. *Combust. Flame* **1985**, *62*, 193.
(10) Williams, B. A.; Pasternack, L. *Combust. Flames* **1997**, *111*, 87.
(11) Kruse, T.; Roth, P. *Int. J. Chem. Kinet.* **1999**, *31*, 11.
(12) Becker, K. H.; Dinis, C. M. F. *Ber.-Bergische University, Gesamthochsch. Wuppertal, Fachbereich 9, Phys. Chem.* **1998**, *45*, 1 (in German).
(13) Becker, K. H.; Donner, B.; Dinis, C. M. F.; Geiger, H.; Schmidt, F.; Wiesen, P. Z. *Phys. Chem.* **2000**, *214*, 503.
(14) Ristanovic, A.; Fernandez, A.; Fontijn, A. *J. Phys. Chem. A* **2002**, *106*, 8291.
(15) Chase, M. W., Jr., Ed. *NIST-JANAF Thermochemical Tables*, 4th ed.; Journal of Physical Chemistry Reference Data, Monograph 9; American Chemical Society: Washington, DC, 1998.
(16) Huber, K. P.; Herzberg, G. *Molecular Spectra and Molecular Structure. IV Constants of Diatomic Molecules*; Van Nostrand Reinhold: NewYork, 1979; p 154.
(17) According to Kruse and Roth, *J. Phys. Chem. A* **1997**, *101*, 2138, the $\Delta H°_{298}$ values used for C_2 in this paper may have to be reduced by about 5 kcal mol^{-1}.
(18) The most likely C_2N product of C_2 collisions with NO is CCN. Apparently, $\Delta H°_f$ for that species is unknown.
(19) Choi, H.; Mordaunt, D. H.; Bise, R. T.; Taylor, T. R.; Neumark, D. M. *J. Chem. Phys.* **1998**, *108*, 4070.
(20) Frisch, M. J.; Trucks, G. W.; Schlegel, H. B.; Scuseria, G. E.; Robb, M. A.; Cheeseman, J. R.; Zakrzewski, V. G.; Montgomery, J. A., Jr.; Stratmann, R. E.; Burant, J. C.; Dapprich, S.; Millam, J. M.; Daniels, A. D.; Kudin, K. N.; Strain, M. C.; Farkas, O.; Tomasi, J.; Barone, V.; Cossi, M.; Cammi, R.; Mennucci, B.; Pomelli, C.; Adamo,C.; Clifford, S.; Ochterski, J.; Petersson, G. A.; Ayala, P. Y.; Cui, Q.; Morokuma, K.; Malick, D. K.; Rabuck, A. D.; Raghavachari, K.; Foresman, J. B.; Cioslowski, J.; Ortiz, J. V.; Stefanov, B.; Liu, B. G.; Liashenko, A.; Piskorz, P.; Komaromi, I.; Gomperts, R.; Martin, R. L.; Fox, D. J.; Keith, T.; Al-Laham, M. A.; Peng, C. Y.; Nanayakkara, A.; Gonzalez, C.; Challacombe, M.; Gill, P. M. W.; Johnson, B.; Chen, W.; Wong, M. W.; Andres, J. L.; Gonzalez, C.; Head-Gordon, M.; Replogle, E. S.; Pople, J. A. *Gaussian 98*, revision A.7; Gaussian, Inc., Pittsburgh, PA, 1998.